UC Irvine
UC Irvine Previously Published Works

Title

An EPR and VTVH MCD spectroscopic investigation of the nitrogenase assembly protein NifB.

Permalink

Journal

ISSN

Authors

Rupnik, Kresimir
Rettberg, Lee
Tanifuji, Kazuki
et al.

Publication Date

2021-06-01

DOI

Peer reviewed

An EPR and VTVH MCD Spectroscopic Investigation of the Nitrogenase Assembly Protein NifB

Kresimir Rupnik[#], **Lee Rettberg**[†], **Kazuki Tanifuji**[†], **Johannes G. Rebelein**[§], **Markus W. Ribbe**[†,‡], **Yilin Hu**[†], **Brian J. Hales**[#]

[†]Department of Molecular Biology and Biochemistry, University of California, Irvine, CA 92697-3900

[‡]Department of Chemistry, University of California, Irvine, CA 92697-2025

[§]Max Planck Institute for Terrestrial Microbiology Marburg, Karl-von-Frisch-Strasse 10, 35043 Marburg, Germany

[#]Department of Chemistry, Louisiana State University, Baton Rouge, LA 70803

Abstract

NifB, a radical SAM enzyme, catalyzes the biosynthesis of the *L* cluster (Fe_8S_9C), a structural homolog and precursor to the nitrogenase active-site *M* cluster ([$MoFe_7S_9C$•*R-homocitrate*]). Sequence analysis shows that NifB contains the CxxCxxxC motif that is typically associated with the radical SAM cluster ([Fe_4S_4]$_{SAM}$) involved in the binding of *S*-adenosylmethionine (SAM). In addition, NifB houses two transient [Fe_4S_4] clusters (*K* cluster) that can be fused into an 8Fe *L* cluster concomitant with the incorporation of an interstitial carbide ion, which is achieved through radical SAM chemistry initiated at the [Fe_4S_4]$_{SAM}$ cluster upon its interaction with SAM. Here, we report a VTVH MCD/EPR spectroscopic study of the *L* cluster biosynthesis on NifB, which focuses on the initial interaction of SAM with [Fe_4S_4]$_{SAM}$ in a variant NifB protein (*Ma*NifB^{SAM}) containing only the [Fe_4S_4]$_{SAM}$ cluster and no *K* cluster. Titration of *Ma*NifB^{SAM} with SAM reveals that [Fe_4S_4]$_{SAM}$ exists in two forms, labeled [Fe_4S_4]$^+_{SAM}$*A* and [Fe_4S_4]$^{2+}_{SAM}$*B*. It is proposed that these forms are involved in the synthesis of the *L* cluster. Of the two cluster types, only [Fe_4S_4]$^{2+}_{SAM}$*B* initially interacts with SAM, resulting in the generation of *Z*, an $S = ½$ paramagnetic [Fe_4S_4]$_{SAM}$/SAM complex.

Graphic Abstract

Radical SAM enzymes are ubiquitous in Nature.[1] These enzymes form a superfamily that utilize the interaction of S-adenosylmethionine (SAM) with a $[Fe_4S_4]^+$ cluster to generate a 5'-deoxyadenosyl radical (5'-dA•). In most of these reactions, the highly reactive 5'-dA• radical undergoes subsequent reactions, typically H-atom abstraction, with a variety of substrates. One interesting radical SAM reaction involves the biosynthesis of the highly complex metallocofactor (*M* cluster), which serves as the active site of nitrogenase— an enzyme responsible for biological nitrogen fixation.[2–5] The *M* cluster ($[MoFe_7S_9C•R\text{-}homocitrate]$) is comprised of $[MoFe_3S_3]$ and $[Fe_4S_3]$ clusters bridged by three μ_2-sulfides, and it also contains an interstitial μ_6–carbide ion and an organic homocitrate entity at its Mo end.[6–9]

The biosynthesis of the *M* cluster has long been of interest to chemists and biochemists alike because of the complexity and uniqueness of this cofactor. Formation of the *M* cluster is believed to begin with the action of NifS (a cysteine desulfurase) and NifU (a scaffold protein), which catalyze the formation of $[Fe_4S_4]$ clusters.[10–13] Subsequently, a pair of $[Fe_4S_4]$ clusters (designated the *K* cluster) is transferred to NifB, where they are fused into an 8Fe *L* cluster ($[Fe_8S_9C]$) concomitant with the insertion of a carbide ion into the central cavity of the cluster. The *L* cluster is then transferred to NifEN, another scaffold protein, where one of its terminal *Fe* atoms is replaced by *Mo* and *R*-homocitrate to generate a fully-complemented *M* cluster.[11]

Like most members of the radical SAM enzyme superfamily, NifB contains a characteristic CxxCxxxC motif that is involved in ligating three *Fe* atoms of a $[Fe_4S_4]$ cluster.[1] The fourth *Fe* atom of this permanent $[Fe_4S_4]$ cluster (designated $[Fe_4S_4]_{SAM}$) remains free and serves as the primary site for SAM binding. In addition, NifB contains extra ligands for the coordination of a transient pair of $[Fe_4S_4]$ clusters (*K* cluster), which can be coupled into an 8*Fe* core (*L* cluster) of the M-cluster concomitant with carbide insertion. Previously, the NifB protein from a mesophilic methanogen, *Methanosarcina acetivorans*, was heterologously expressed in *Escherichia coli*.[14] A monomer of ~38 kDa, this NifB

protein (designated *Ma*NifB) was shown to be fully active in converting the **K** cluster to an **L** cluster upon incubation with SAM.[14] Recently, the presence of a permanent $[Fe_4S_4]_{SAM}$ cluster and the transient **K**-cluster on NifB was further confirmed by combined biochemical and spectroscopic investigations, which led to the assignment of three Cys ligands to each $[Fe_4S_4]$ cluster, as well as a fourth His ligand to one of the $[Fe_4S_4]$ modules of the **K** cluster, on *Ma*NifB.[15]

Despite the recent progress toward understanding the functionality of NifB, the mechanistic details of the biosynthesis of **L** cluster on NifB remain elusive. Here, we report a study that uses a combination of variable-temperature, variable-field magnetic circular dichroism (VTVH MCD) and electron paramagnetic resonance (EPR) spectroscopies to study the first step in the **L** cluster synthesis, namely, the interaction of SAM with the permanent $[Fe_4S_4]_{SAM}$ cluster on NifB. Our study reveals that the $[Fe_4S_4]_{SAM}$ cluster exists in two different forms and that one of the forms initially binds SAM and induces a unique inversion of the MCD spectrum of the $[Fe_4S_4]_{SAM}$ cluster on NifB. This previously unobserved effect suggests an interaction between SAM and the $[Fe_4S_4]_{SAM}$ cluster, which primes the complex for radical formation in the presence of substrate. These results form a basis for further investigation into the unique radical chemistry employed by NifB for the biosynthesis of the elusive nitrogenase cofactor.

RESULTS

To understand the initial mechanism of **L** cluster synthesis and, in particular, the role of the NifB-associated $[Fe_4S_4]_{SAM}$ cluster in this process, a variant *Ma*NifB protein, *Ma*NifB^{SAM}, which contains only the $[Fe_4S_4]_{SAM}$ cluster and no **K** cluster, was constructed by mutating the Cys ligands of the **K** cluster to Ala.[15] Unlike the wild-type *Ma*NifB, *Ma*NifB^{SAM} should have the ability to interact with SAM but is unable to carry out subsequent reactions that involve the **K** cluster,[14] thereby allowing the first step of the NifB-catalyzed reaction to be investigated without interference of the subsequent steps in this complicated process.

Based on the previous observation that the formation of **L** cluster on NifB maximizes at 40 mmol*dm^{-3} SAM,[16] the X-band EPR spectrum of *Ma*NifB^{SAM} was recorded in the presence of SAM concentrations ranging from 0 to 40 mmol*dm^{-3} (Figure 1). In the absence of SAM,[17–19] *Ma*NifB^{SAM} (designated *Ma*NifB$_A^{SAM}$) exhibits a near-axial EPR spectrum ($g = 2.017, 1.924, 1.910$; $\sigma = 0.030, 0.020, 0.070$).[15] Addition of SAM induces gradual changes in the spectrum, consistent with an interaction of SAM with $[Fe_4S_4]_{SAM}$, as has been observed for other radical-SAM enzymes.[1]

To aid the interpretation of the EPR spectra, simulations were performed. These simulations revealed that two major signals (Figure 2), one very similar to the original spectrum of *Ma*NifB$_A^{SAM}$ (called *Ma*NifB$_A^{SAM*}$ with $g = 2.017, 1.923, 1.885$; $\sigma = 0.030, 0.023, 0.085$) and the other of an unknown cluster **Z** ($g = 1.982, 1.884, 1.866$; $\sigma = 0.020, 0.032, 0.032$), were needed to closely simulate all of the spectra. Based on the results from simulations, the relative EPR spin concentrations (from the simulations) of the two signals that contribute to each spectrum are plotted in Figure 3.

The electronic structure of the cluster species on $Ma\text{NifB}_A^{SAM}$ was further probed by VTVH MCD spectroscopy. As expected, the VTVH MCD spectrum of $Ma\text{NifB}_A^{SAM}$ (Figure 4), as expected, exhibits the classic features associated with a $[Fe_4S_4]^+$ cluster, namely, a broad first derivative-like curve centered around 600 nm.[20–22] It is important to note the absence of detectable spectral components normally associated with $[Fe_2S_2]^+$ or $[Fe_3S_4]^{0/1+}$ clusters,[22–23] which have been previously detected in preparations of other radical SAM enzymes.[24] The decrease in the spectral intensity of $Ma\text{NifB}_A^{SAM}$ with increasing temperature (Figure 4) is consistent with the MCD spectrum being assigned to a paramagnetic center. Magnetization curves of $Ma\text{NifB}_A^{SAM}$ (Figure SF1) further suggest a paramagnetic ($S = \frac{1}{2}$) spectrum and predict an underlying B-term due to the presence of a diamagnetic component.

The MCD spectra of $Ma\text{NifB}^{SAM}$ (Figure 5) were also recorded for the EPR samples shown in Figure 1. What is unexpected and unusual is the general decrease of the intensity of the entire MCD spectrum with increasing concentration of SAM. This trend is opposite to the increase of the total spin concentration (green line in Figure 3).

The EPR spectral simulations (Figures 2 and SF1) have approximated the relative concentration of $Ma\text{NifB}_A^{SAM}$ at each concentration of SAM (Figure 3). Since the MCD spectrum of $Ma\text{NifB}_A^{SAM}$ is already known (Figure 4), it follows that any underlying residual SAM-induced MCD spectra can be derived from the total spectrum (Figure 5). Figure 6 shows the derived SAM-induced contributions to the MCD spectra at each concentration of SAM.

DISCUSSION

The EPR spectral data presented herein clearly indicate that SAM interacts with the $[Fe_4S_4]_{SAM}$ cluster in $Ma\text{NifB}^{SAM}$, as has been observed for other radical-SAM enzymes.[1] Spectral simulations reveal only a small near-linear decrease of the EPR spin concentration of the as-isolated paramagnetic cluster in $Ma\text{NifB}_A^{SAM}$ yet a much larger increase of the EPR spin concentration of the newly-formed **Z** species with increasing concentration of SAM (Figure 3). This suggests that **Z** is not solely directly formed from $Ma\text{NifB}_A^{SAM}$. Consistent with these results, the total experimental EPR spin concentration, i.e., **Z** $+ Ma\text{NifB}_A^{SAM}$ (green data in Figure 3), increases dramatically with increasing concentration of SAM. If **Z** was directly formed from $Ma\text{NifB}_A^{SAM}$, the total spin concentration would remain constant.

Simulations also show an interesting effect of SAM on the EPR spectrum of the cluster in the parent $Ma\text{NifB}_A^{SAM}$. Specifically, in the presence of SAM the EPR spectrum of $Ma\text{NifB}_A^{SAM}$ is slightly shifted to a new form called $Ma\text{NifB}_A^{SAM*}$ (see Figure SF2). This SAM-induced EPR spectral shift of the cluster in the parent protein is not unique to $Ma\text{NifB}^{SAM}$ and has been observed for other radical-SAM enzymes.[25] The origin of

the shift is unknown but the fact that the shift is small suggests a distant, non-bonding interaction between SAM and the cluster in the parent protein.

Since there is only one $[Fe_4S_4]$ cluster in MaNifB^{SAM}, it has to be that cluster that eventually gives rise to $\mathbf{Z}$. To get around this apparent contradiction, the as-isolated MaNifB^{SAM} is proposed to exist as a mixture of two forms, labeled MaNifB$_A^{SAM}$ and MaNifB$_B^{SAM}$. In this proposal, MaNifB$_A^{SAM}$ contains cluster $[Fe_4S_4]_{SAM}^+A$, which is EPR- and MCD-active (Figures 1 and 4, respectively), while MaNifB$_B^{SAM}$, in the absence of SAM, contains cluster $[Fe_4S_4]_{SAM}^{2+}B$, which is EPR-silent. This proposal is consistent with the metal and spectral analysis of MaNifB^{SAM},[15] which shows that it contains 3.1 ± 0.4 Fe/protein (78% of the expected occupancy of 4 Fe/protein) and an $S = \frac{1}{2}$ spin concentration of 0.38 ± 0.05 per protein. Given the $S = \frac{1}{2}$ spin concentration of approximately 0.5 per protein at 100% cluster occupancy, approximately half of the Fe atoms in MaNifB^{SAM} are associated with a paramagnetic cluster (i.e., $[Fe_4S_4]_{SAM}^+A$) with an $S = \frac{1}{2}$ ground state while the remainder half of the Fe atoms are associated with and EPR-silent, diamagnetic cluster (i.e., $[Fe_4S_4]_{SAM}^{2+}B$). The existence of two forms of MaNifB^{SAM} may arise from slight structural differences that cause the two cluster forms to have different midpoint potentials such that the $[Fe_4S_4]_{SAM}^{2+}B$ cluster is not reduced in the presence of dithionite.

It is additionally proposed that SAM predominantly interacts with $[Fe_4S_4]_{SAM}^{2+}B$ to produce the EPR-active $\mathbf{Z}$, or

$$[Fe_4S_4]_{SAM}^{2+}B \xrightarrow{SAM} \mathbf{Z} \tag{1}$$

This is consistent with the increase in total spin concentration (green line in Figure 3) with increasing concentration of SAM. $[Fe_4S_4]_{SAM}^+A$ may also be used to generate $\mathbf{Z}$. However, because the EPR spin concentration of $[Fe_4S_4]_{SAM}^+A$ appears to decrease only slightly upon addition of increasing concentrations of SAM, $[Fe_4S_4]_{SAM}^+A$ is likely not the dominant reactant that gives rise to $\mathbf{Z}$.

What is $\mathbf{Z}$? $\mathbf{Z}$ exhibits a near-axial EPR spectrum that is similar to the published spectra of a variety of radical SAM enzymes with SAM bound to them (see Table 2 in Reference 1), suggesting a similarity of the structure of $\mathbf{Z}$ to those of the SAM-bound cluster species in these enzymes. The structures of several enzymes following treatment with SAM have been studied using a combination of electron nuclear double resonance (ENDOR) spectroscopy and x-ray crystallography. For example, spectroscopic studies of the radical SAM enzymes pyruvate formate-lyase activating enzyme (PFL-AE)[23, 26–29] and lysine 2,3-aminomutase (LAM)[30] show binding of SAM as a coordination complex, where the amino and carboxyl units of SAM chelate the unique, open Fe site of the $[Fe_4S_4]_{SAM}^+$ cluster, and these

observations have been further confirmed by x-ray crystallographic determinations.[31] Figure 7 shows the crystal structure of PFL-AE (PDB ID 3CB8),[32] which is proposed here to be similar to the structure of complex **Z**.

The MCD spectra of the SAM-treated *Ma*NifB^{SAM} samples (Figure 6) are also noteworthy as they represent the MCD spectra of the components other than $[Fe_4S_4]^+_{SAM}A$ in the system that are induced by SAM. In other words, they represent the composite spectra of **Z** and any additional new diamagnetic (i.e., *B*-terms) and paramagnetic components. While the general overall shape of all these difference spectra are similar (see below), they are not identical and exhibit small changes with increasing concentration of SAM. This observation suggests that the spectra do not represent a single component (i.e., **Z**). Diamagnetic components (i.e., *B*-terms) exhibit only small MCD spectra at low temperature compared with paramagnetic components (i.e., *C*-terms) and, therefore, will contribute little to the total MCD spectrum. While there are no EPR spectral indications of the presence of additional paramagnetic species, their presence cannot be completely ruled out. For example, **Z** may be predominantly generated by $[Fe_4S_4]^+_{SAM}B$ (Equation 1), while the small, near linear decrease in the EPR spin concentration of $[Fe_4S_4]^+_{SAM}A$ with increasing concentration of SAM could correspond to the formation of an additional unknown EPR-silent species. Regardless, the MCD spectra of SAM-treated *Ma*NifB^{SAM} samples are likely dominated by the spectrum of **Z**.

Another unusual property of the difference spectra in Figure 5 is that they don't exhibit the characteristic, first derivative-like structure observed for typical $[Fe_4S_4]^+$ clusters (see above for discussion of the results shown in Figure 4), even though **Z** is presumably a major contributor to these spectra. This observation suggests that binding of the organic SAM molecule to the cluster in *Ma*NifB^{SAM} may involve an interaction different than that typically observed for ordinary amino acid ligands,[33] and that such a difference changes the MCD spectrum of *Ma*NifB^{SAM}.

Finally, the existence of two forms of the $[Fe_4S_4]_{SAM}$ cluster in *Ma*NifB^{SAM} may have mechanistic relevance to **L** cluster synthesis, which involves two different radical SAM reactions. The first reaction involves the methylation of the **K** cluster, while the second reaction involves hydrogen atom abstraction from the added methyl group, eventually leading to the formation of the central carbide atom of the **L** cluster.[2, 15] Since SAM initially binds to the $[Fe_4S_4]^{2+}_{SAM}B$ cluster, that cluster form is likely instrumental in the first reaction, namely, methylation of the **K** cluster. Following methylation, the cluster is proposed to be converted to the $[Fe_4S_4]^+_{SAM}A$ form, which interacts with SAM to generate the 5'-dA• radical for the second reaction, namely, hydrogen atom abstraction of the **K** cluster-bound methyl group. As such, *Ma*NifB is proposed to oscillate between the two cluster forms during the synthesis of the **L** cluster. Obviously, the existence of two cluster types in the variant protein is unexpected and a similar EPR/MCD spectroscopic study must be undertaken with the wild-type enzyme.

CONCLUSION

In summary, the EPR and MCD spectroscopic data presented herein suggest that the $[Fe_4S_4]_{SAM}$ cluster in the *FeS*-reconstituted *Ma*NifB^{SAM} exists in two different forms, $[Fe_4S_4]^+_{SAM}A$ and $[Fe_4S_4]^{2+}_{SAM}B$, which may be related to the two different radical SAM reactions involved in the synthesis of the L cluster. In this proposal, SAM initially interacts with $[Fe_4S_4]^{2+}_{SAM}B$ at low concentrations to produce **Z**, a proposed $\left([Fe_4S_4]^+_{SAM}B/SAM\right)$ complex. Why SAM preferentially interacts with $[Fe_4S_4]^{2+}_{SAM}B$ and not $[Fe_4S_4]^+_{SAM}A$ is unknown. However, it has been shown that the as-isolated radical SAM enzymes PFL-AE and LAM also contain an oxidized $[Fe_4S_4]^{2+}$ cluster, which, upon binding of SAM, forms a $[Fe_4S_4]^{2+}/SAM$ complex. This complex is subsequently reduced to a paramagnetic complex, $[Fe_4S_4]^+/SAM$, like that proposed for **Z**.[23, 34] The *in vitro* reduction of the cluster from $\left([Fe_4S_4]^{2+}_{SAM}B - SAM\right)$ to $\left([Fe_4S_4]^+_{SAM}B - SAM\right)$ is likely carried out by an exogenous reductant, such as dithionite, and it occurs because SAM binding has been shown to change the redox midpoint, making the reduced $[Fe_4S_4]^+$ cluster the favored state.[34]

Supplementary Material

Refer to Web version on PubMed Central for supplementary material.

Funding

REFERENCES

1. Broderick JB; Duffus BR; Duschene KS; Shepard EM, Radical S-Adenosylmethionine Enzymes. Chem. Rev2014, 114, 4229–4317. [PubMed: 24476342]

2. Hu Y; Ribbe MW, Biosynthesis of the Metalloclusters of Nitrogenases. Annu. Rev. Biochem2016, 85, 455–483. [PubMed: 26844394]

3. Burgess BK; Lowe DJ, Mechanism of Molybdenum Nitrogenase. Chem. Rev1996, 96, 2983–3011. [PubMed: 11848849]

4. Hoffman BM; Lukoyanov D; Yang Z-Y; Dean DR; Seefeldt LC, Mechanism of Nitrogen Fixation by Nitrogenase: The Next Stage. Chem. Rev2014, 114 (8), 4041–4062. [PubMed: 24467365]

5. Hoffman BM; Lukoyanov D; Dean DR; Seefeldt LC, Nitrogenase: A Draft Mechanism. Acc. Chem. Res2013, 46 (2), 587–595. [PubMed: 23289741]

6. Rees DC; Kim J; Woo D, X-ray Crystal Structure of the Nitrogenase Molbdenum-Iron Protein from Clostridium pasteurianum at 3.0-Å Resolution. Biochemistry1993, 32, 7104–7115. [PubMed: 8393705]

7. Einsle O; Tezca FA; Andrade SLA; Schmid B; Yoshida M; Howard JB; Rees DC, Nitrogenase MoFe-Protein at 1.16 Å Resolution: A Central Ligand in the FeMo-Cofactor. Science2002, 297, 1696–1700. [PubMed: 12215645]

8. Spatzal T; Aksoyoglu M; Zhand L; Andrade SLA; Schleicher E; Weber S; Rees DC; Einsle O, Evidence for Interstitial Carbon in Nitrogenase FeMo Cofactror. Science2011, 334, 940. [PubMed: 22096190]

9. Lancaster KM; Roemelt M; Ettenhuber P; Hu Y; Ribbe MW; Neese F; Bergmann U; DeBeer S, X-Ray Emission Spectroscopy Evidences a Central Carbon in the Nitrogenase Iron-Molybdenum Cofactor. Science2011, 334, 974–977. [PubMed: 22096198]

10. Sickerman NS; Ribbe MW; Hu Y, Nitrogenase Cofactor Assembly: An Elemental Inventory. Acc. Chem. Res2017, 50 (11), 2834–2841. [PubMed: 29064664]

11. Hu Y; Corbett MC; Fay AW; Webber JA; Hodgson KO; Hedman B; Ribbe MW, FeMo cofactor maturation on NifEN. Proc. Natl. Acad. Sci. U. S. A2006, 103 (46), 17119–17124. [PubMed: 17050696]

12. Yoshizawa J; Blank MA; Fay AW; Lee CC; Wiig JA; Hu Y; Hodgson KO; Hedman B; Ribbe MW, Optimization of FeMoco Maturation on NifEN. J. Am. Chem. Soc2009, 131, 9321–9325. [PubMed: 19514721]

13. Kaiser JT; Hu Y; Wiig JA; Rees DC; Ribbe MW, Structure of Precursor-Bound NifEN: A Nitrogenase FeMo Cofactor Maturase/Insertase. Science2011, 331, 91–94. [PubMed: 21212358]

14. Fay AW; Wiig JA; Lee CC; Hu Y, Identification and characterization of functional homologs of nitrogenase cofactor biosynthesis protein NifB from methanogens. Proc. Natl. Acad. Sci. U. S. A2015, 112 (48), 14829–14833. [PubMed: 26627238]

15. Rettberg LA; Wilcoxen J; Lee CC; Stiebritz MT; Tanifuji K; Britt RD; Hu Y, Probing the coordination and function of Fe_4S_4 modules in nitrogenase assembly protein NifB. Nat. Comm2018, 9, 2824–2832.

16. Wiig JA; Hu Y; Ribbe MW, NifEN-B Complex of *Azotobacter vinelandii* is Fully Functional in Nitrogenase FeMo Cofactor Assembly. Proc. Natl. Acad. Sci. U. S. A2011, 108, 8623–8627. [PubMed: 21551100]

17. Schatz PN; McCaffrey AJ, The Faraday Effect. Q. Rev. Chem. Soc1969, 23, 552–584.

18. Johnson MK; Thomson AJ; Robinson AE; Rao KK; Hall DO, Low-Temperature Magnetic Circular Dichroism Spectra and Magnetisation Curves of 4Fe Clusters in Iron-Sulphur Proteins from *Chromatium* and *Clostridium pasteurianum*. Biochim. Biophys. Acta1981, 667, 433–451. [PubMed: 6260220]

19. Johnson MK, CD and MCD Spectroscopy. In Physical Methods in Bioinorganic Chemistry, Que Jr., Ed. University Science Books: Sausalito, 2000; pp 233–286.

20. Conover RC; Kowal AT; Fu W; Park J-B; Aono S; Adams MWW; Johnson MK, Spectroscopic Characterization of the Novel Iron-Sulfur Cluster in *Pyrococcus furiosus* Ferredoxin. J. Biol. Chem1990, 265 (15), 8533–8541. [PubMed: 2160461]

21. Onate YA; Finnegan MG; Hales BJ; Johnson MK, Variable Temperature Magnetic Circular Dichroism Studies of Reduced Nitrogenase Iron Proteins and [4Fe-4S]$^+$ Synthetic Analog Clusters. Biochim. Biophys. Acta1993, 1164, 113–123. [PubMed: 8329442]

22. Johnson MK; Robinson AE; Thomson AJ, Low-Temperature Magnetic Circular Dichroism Studies of Iron-Sulfur Proteins. In Iron-Sulfur Proteins, Spiro TG, Ed. Wiley-Interscience: New York, NY, 1982; pp 367–406.

23. Broderick JB; Duderstadt RE; Fernandez DC; Wojtuszewski K; Henshaw TF; Johnson Michael K, Pyruvate Formate-Lyase Activating Enzyme Is an Iron-Sulfur Protein. J. Am. Chem. Soc1997, 119, 7396–7397.

24. Broderick JB; Henshaw TF; Cheek J; Wojtuszewski K; Smith SR; Trojan MR; McGhan RM; Kopf A; Kibbey M; Broderick WE, Pyruvate Formate-Lyase-Activating Enzyme: Strictly Anaerobic Isolation Yields Active Enzyme Containing a [3Fe–4S]. Biochem. Biophys. Res. Commun2000, 269, 451–456. [PubMed: 10708574]

25. Kathirvelu V; Perche-Letuvee P; Latour J-M; Atta M; Forouhar F; Gambarelli S; Garcia-Serres R, Spectroscopic evidence for cofactor–substrate interaction in the radical-SAM enzyme TYW1. Dalton Transactions2017, 46, 13211–13219. [PubMed: 28640310]

26. Walsby CJ; Hong W; Broderick WE; Cheek J; Ortillo D; Broderick JB; Hoffman BM, Electron-Nuclear Double Resonance Spectroscopic Evidence That S-Adenosylmethionine Binds in Contact with the Catalytically Active [4Fe-4S]+ Cluster of Pyruvate Formate-Lyase Activating Enzyme. J. Am. Chem. Soc2002, 124 (12), 3143–3151. [PubMed: 11902903]

27. Horitani M; Byer AS; Shisler K; Chandra T; Broderick JB; Hoffman BM, Why Nature Uses Radical SAM Enzymes so Widely: Electron Nuclear Double Resonance Studies of Lysine 2,3 Aminomutase Show the 5′-dAdo• "Free Radical" Is Never Free. J. Am. Chem. Soc2015, 137, 7111–7121. [PubMed: 25923449]

28. Horitani M; Shisler K; Broderick WE; Hutcheson RU; Duschene KS; Marts AR; Hoffman BM; Broderick JB, Radical SAM catalysis via an organometallic intermediate with an Fe–[5′-C]-deoxyadenosyl bond. Science2016, 352 (6287), 822–825. [PubMed: 27174986]

29. Broderick WE; Hoffman BM; Broderick JB, Mechanism of Radical Initiation in the Radical S-Adenosyl-L-methionine Superfamily. Acc. Chem. Res2018, 51, 2611–2619. [PubMed: 30346729]

30. Chen D; Walsby CJ; Hoffman BM; Frey PA, Coordination and Mechanism of Reversible Cleavage of S-Adenosylmethionine by the [4Fe-4S] Center in Lysine 2,3-Aminomutase. J. Am. Chem. Soc2003, 125, 11788–11789. [PubMed: 14505379]

31. Vey JL; Drennan CL, Structural Insights into Radical Generation by the Radical SAM Superfamily. Chem. Rev2011, 111 (2487–2506). [PubMed: 21370834]

32. Vey JL; Yang Z-Y; Li M; Broderick WE; Broderick JB; Drennan CL, Structural basis for glycyl radical formation by pyruvate formate-lyase activating enzyme. Proceedings of the National Academy of Sciences2008, 105 (42), 16137–16141.

33. Brereton PS; Duderstadt RE; Staples CR; Johnson Michael K; Adams MWW, Effect of Serinate Ligation at Each of the Iron Sites of the $[Fe_4S_4]$ Cluster of Pyrococcus furiosus Ferredoxin on the Redox, Spectroscopic, and Biological Properties. Biochemistry1999, 38, 10594–10605. [PubMed: 10441157]

34. Frey PA; Hegeman AD; Ruzicka FJ, The Radical SAM Superfamily. Crit. Rev. Biochem. Mol. Biol2008, 43, 63–88. [PubMed: 18307109]
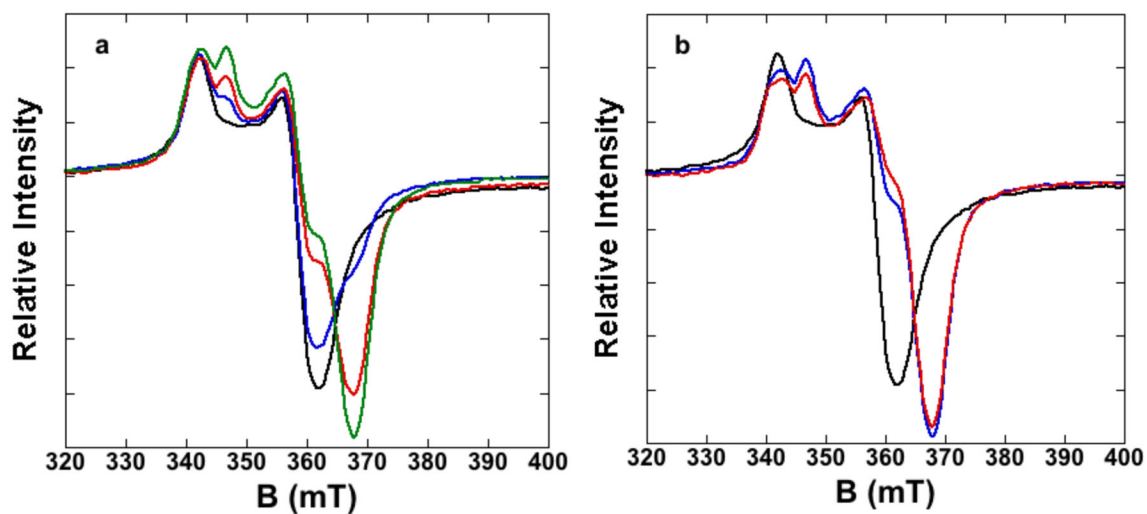
Figure 1.
EPR spectra of *Ma*NifB^{SAM} (black) recorded in the presence of (a) 1 mmol*dm^{-3} (blue) SAM, 5 mmol*dm^{-3} (red) SAM, 10 mmol*dm^{-3} (green) SAM and (b) 20 mmol*dm^{-3} (red) SAM and 40 mmol*dm^{-3} (blue) SAM. All samples had a protein concentration of 14 mg/mL, and the spectra were recorded at a temperature of 20 K, a microwave frequency of 9.678 GHz, a modulation amplitude of 0.5 mT and a microwave power of 5.0 mW.
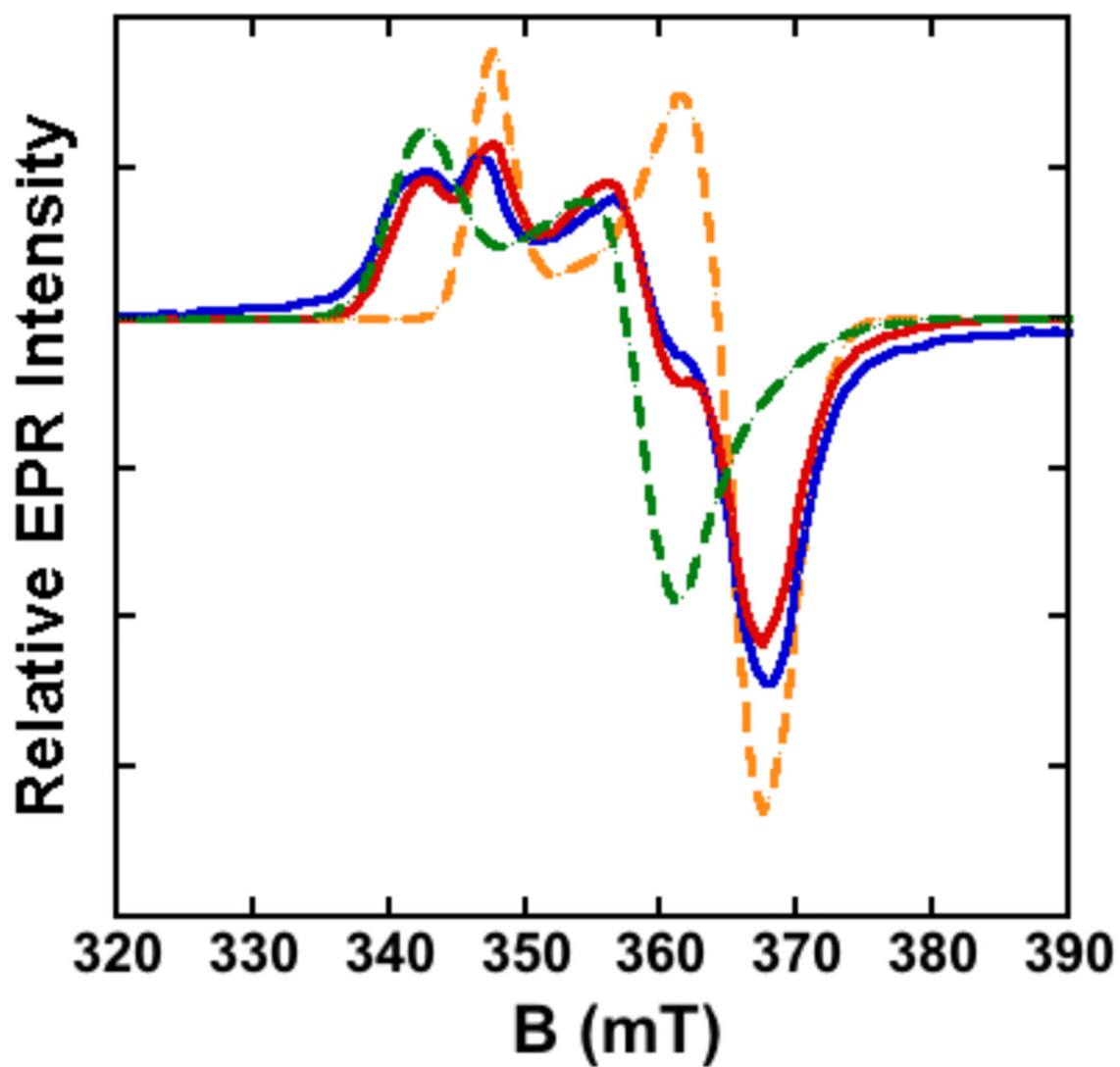
Figure 2.
EPR spectrum of MaNifB^{SAM} (in 15 mmol*dm^{-3} SAM, blue) and its spectral simulation (0.8 MaNifB$_A^{SAM*}$ + 0.5 $\mathbf{Z}$; red) using the simulations of MaNifB$_A^{SAM*}$ (green dashed) and $\mathbf{Z}$ (orange dashed). For reference, all spectra are plotted to have the same relative spin concentration based on double integration.
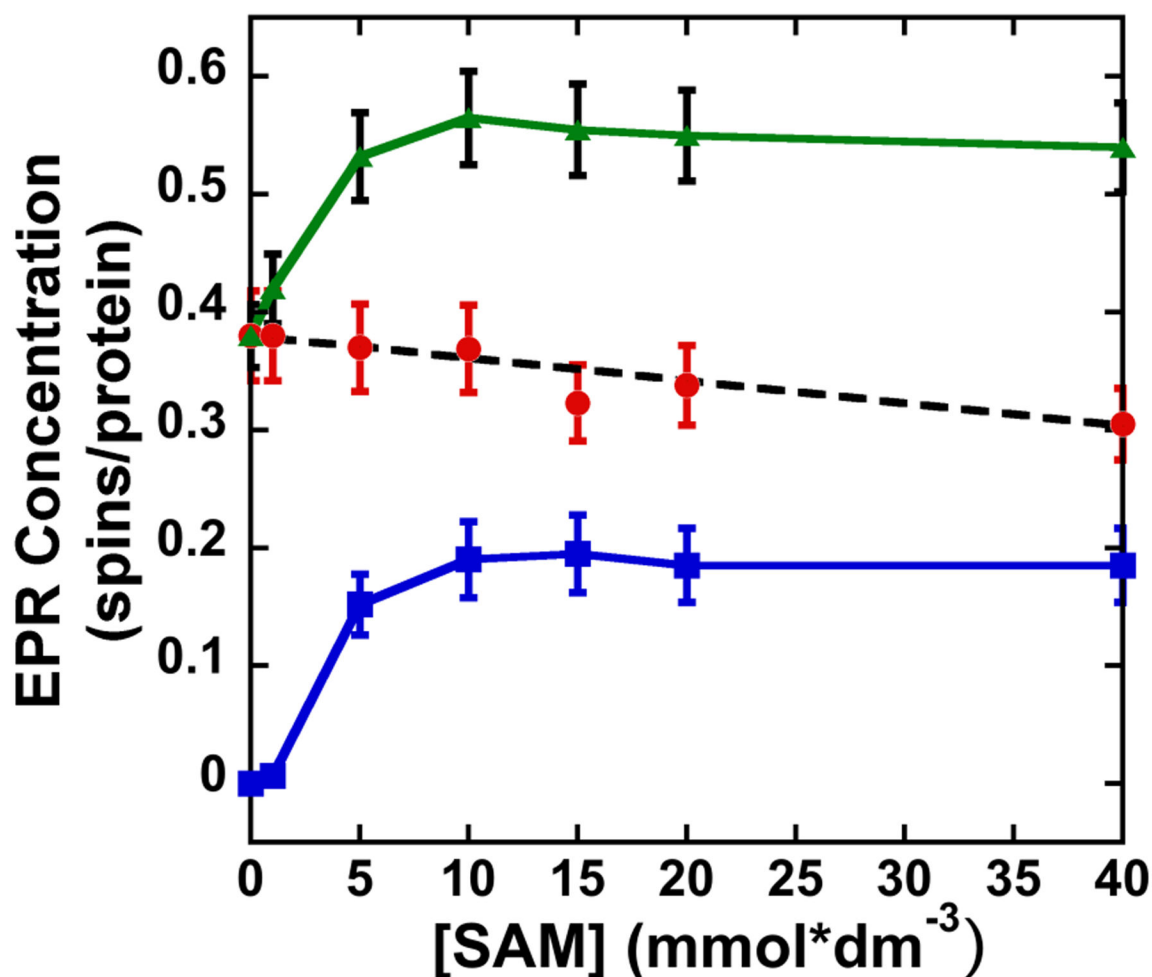
Figure 3.
Spin concentrations, based on the double integration of the EPR spectrum of the $Ma\text{NifB}_A^{SAM}$ sample concentration 0 mmol*dm^{-3}SAM and calculated for the EPR signals of the $Ma\text{NifB}_A^{SAM}$ samples containing > 0 mmol*dm^{-3} SAM from spectral simulations (Figure 1). Spin concentrations of $Ma\text{NifB}_A^{SAM}/Ma\text{NifB}_A^{SAM*}$ are represented by red circles, and those of **Z** are represented by blue squares and line. By contrast, the total spin concentration (plotted as green triangles and line) was determined by double integration of the experimental spectra. Note that the increase in the total spin concentration of the $Ma\text{NifB}_A^{SAM}$ samples with increasing concentration of SAM (green) is consistent with the model proposed in the text. The black dashed line represents a linear approximation of the $Ma\text{NifB}_A^{SAM}/Ma\text{NifB}_A^{SAM*}$ data, while the solid green and blue lines connect the experimental data points and serve as visual aids of the correlation between spin concentrations and concentrations of SAM contained in the $Ma\text{NifB}^{SAM}$ samples.
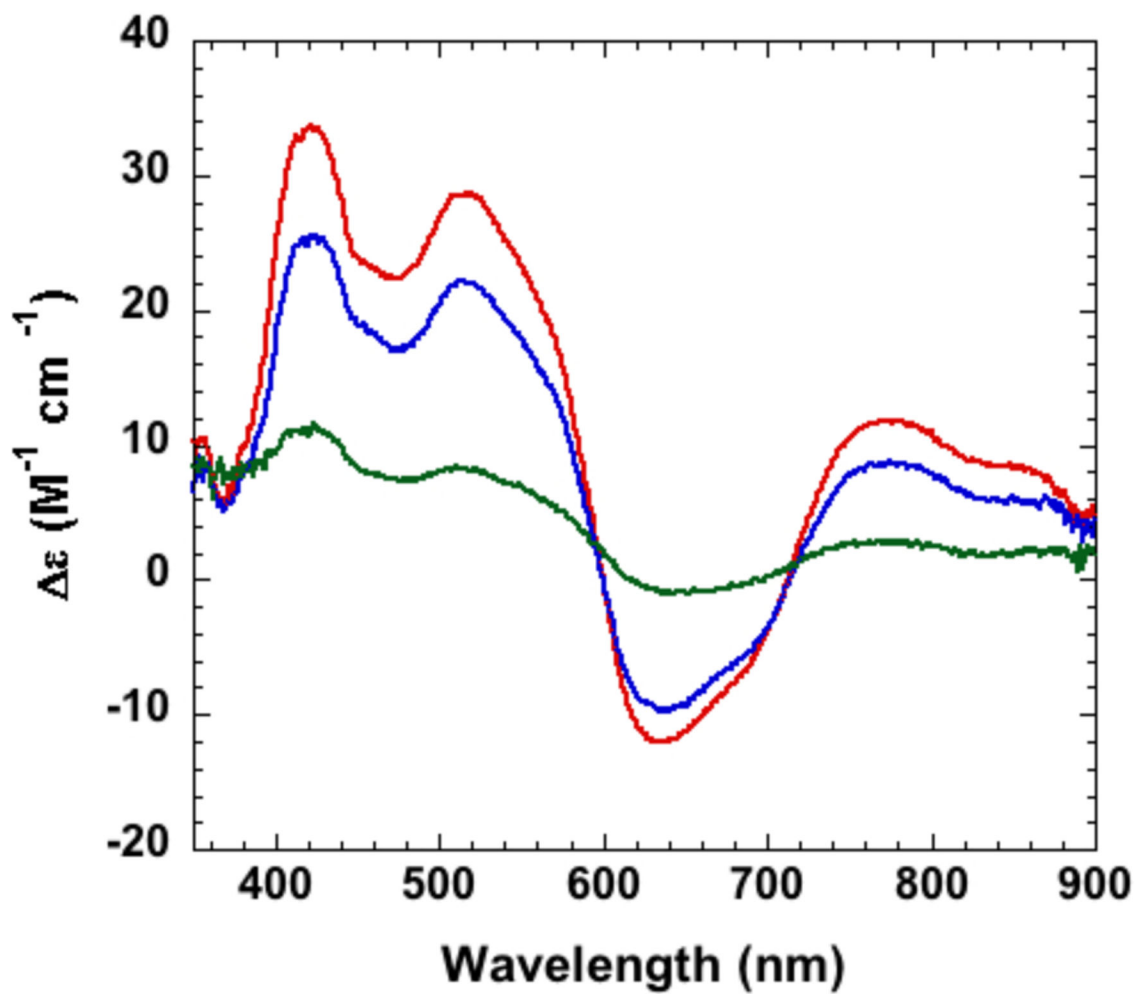
Figure 4.
VTVH MCD spectra of $Ma\mathrm{NifB}_A^{SAM}$ recorded at various temperatures: 1.4 K (red), 4.2 K (blue) and 18 K (green). The protein concentration was 28 mg/mL, and the spectra were recorded at a magnetic field of 6 T.
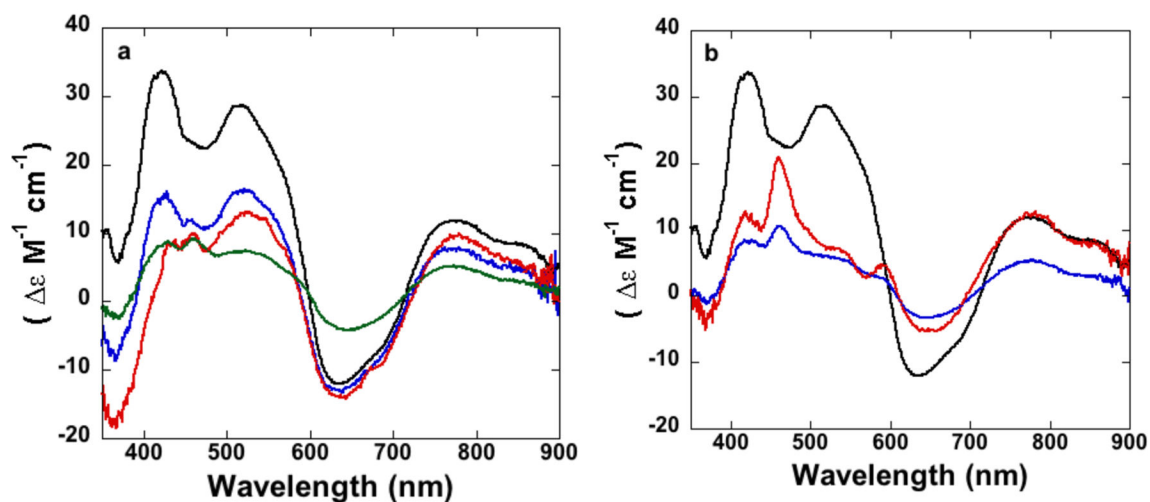
Figure 5.
MCD spectra of MaNifB^{SAM} recorded in the presence of increasing concentrations of SAM from 0 to 40 mmol*dm^{-3}. All protein samples had a concentration of 28 mg/mL, and the spectra were recorded at a magnetic field of 6 T and a temperature of 1.4 K. (a) Spectrum of MaNifB$_A^{SAM}$ (i.e., 0 mmol*dm^{-3} SAM; black) and the spectra of MaNifB^{SAM} in 1 mmol*dm^{-3} (blue), 5 mmol*dm^{-3} (red) and 10 mmol*dm^{-3} (green) SAM. (b) Spectrum of MaNifB$_A^{SAM}$ (black), and spectra of MaNifB^{SAM} in 20 mmol*dm^{-3} (blue) and 40 mmol*dm^{-3} (red) SAM.
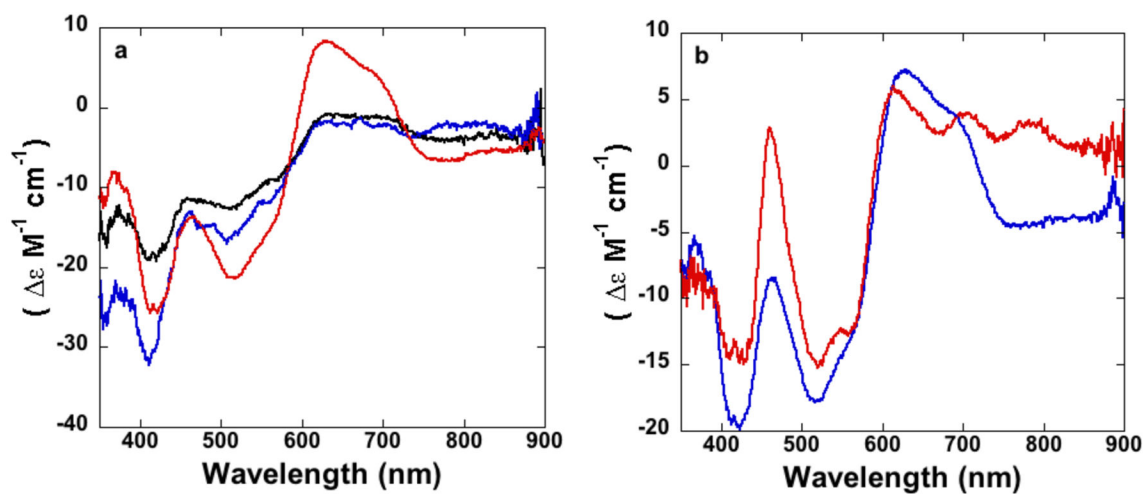
Figure 6.
MCD spectra (at 1.4 K and 6T) obtained by subtracting the MCD spectrum of $Ma\text{NifB}_A^{SAM}$ (determined based on the concentrations from Figure 3) from the total spectrum of $Ma\text{NifB}_A^{SAM}$ at the various SAM concentrations (taken from Figure 4). (a) MCD spectra in 1 mmol*dm^{-3} (black), 5 mmol*dm^{-3} (blue) and 10 mmol*dm^{-3} (red) SAM. (b) MCD spectra in 20 mmol*dm^{-3} (blue) and 40 mmol*dm^{-3} (red) SAM. All protein samples had a concentration of 28 mg/mL.
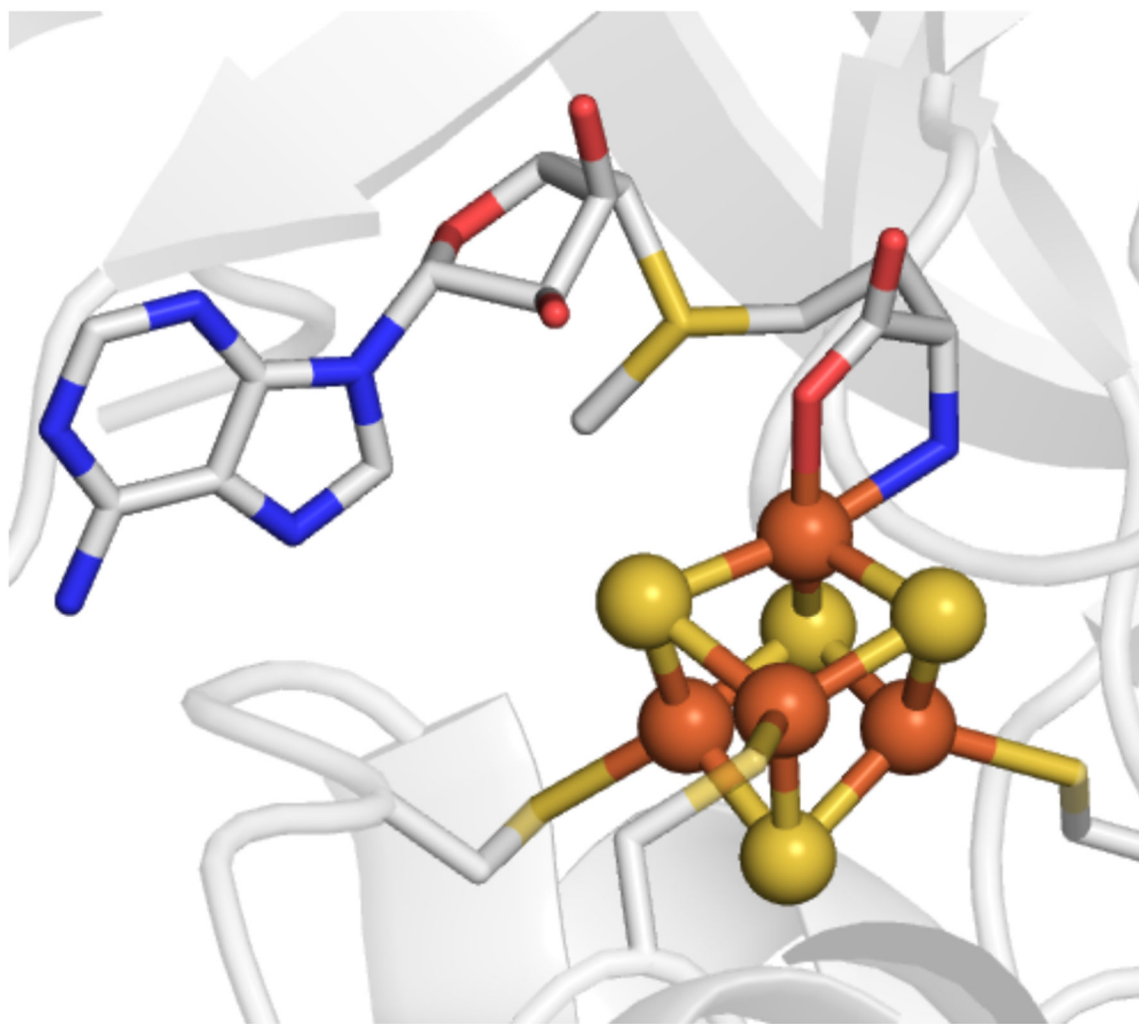
Figure 7.
The EPR spectrum of **Z** is similar to those of SAM interacting with other radical SAM enzymes suggesting a similarity in their structure. An example of one of those structures ($[Fe_4S_4]^+$-SAM) is shown in this figure, which depicts the interaction of the radical SAM enzyme, PFL-AE, interacting with SAM. SAM is shown in the stick presentation and the $[Fe_4S_4]^+$ cluster is shown in the ball-and-stick presentation (PDB ID 3CB8).